Reductive Dissolution of Tl(I)−Jarosite by Shewanella putrefaciens: Providing New Insights into Tl Biogeochemistry

ARTICLE *in* ENVIRONMENTAL SCIENCE & TECHNOLOGY · SEPTEMBER 2012

Impact Factor: 5.33 · DOI: 10.1021/es302292d · Source: PubMed

4 AUTHORS:

Christina M Smeaton
University of Waterloo
9 PUBLICATIONS **38** CITATIONS
SEE PROFILE

Gillian E. Walshe-Langford
University of Tennessee
12 PUBLICATIONS **121** CITATIONS
SEE PROFILE

Brian J Fryer
University of Windsor
199 PUBLICATIONS **5,890** CITATIONS
SEE PROFILE

C. G. Weisener
University of Windsor
57 PUBLICATIONS **838** CITATIONS
SEE PROFILE

Environmental Science & Technology

Article

pubs.acs.org/est

Reductive Dissolution of Tl(I)−Jarosite by *Shewanella putrefaciens*: Providing New Insights into Tl Biogeochemistry

Christina M. Smeaton,*[,†,‡] Gillian E. Walshe,[†,§] Brian J. Fryer,[†] and Christopher G. Weisener[†]

[†]Great Lakes Institute for Environmental Research, University of Windsor, Windsor, Ontario, Canada, N9B 3P4

Supporting Information

ABSTRACT: Thallium (Tl) is emerging as a metal of concern in countries such as China due to its release during the natural weathering of Tl-bearing ore deposits and mining activities. Despite the high toxicity of Tl, few studies have examined the reductive dissolution of Tl mineral phases by microbial populations. In this study we examined the dissolution of synthetic Tl(I)−jarosite, $(H_3O)_{0.29}Tl_{0.71}Fe_{2.74}(SO_4)_2(OH)_{5.22}(H_2O)_{0.78}$, by *Shewanella putrefaciens* CN32 using batch experiments under anaerobic circumneutral conditions. Fe(II) concentrations were measured over time and showed Fe(II) production (4.6 mM) in inoculated samples by 893 h not seen in mineral and dead cell controls. Release of aqueous Tl was enhanced in inoculated samples whereby maximum concentrations in inoculated and cell-free samples reached 3.2 and 2.1 mM, respectively, by termination of the experiment. Complementary batch Tl/*S. putrefaciens* sorption experiments were conducted under experimentally relevant pH (5 and 6.3) at a Tl concentration of 35 μM and did not show significant Tl accumulation by either live or dead cells. Therefore, in contrast to many metals such as Pb and Cd, *S. putrefaciens* does not represent a sink for Tl in the environment and Tl is readily released from Tl−jarosite during both abiotic and biotic dissolution.

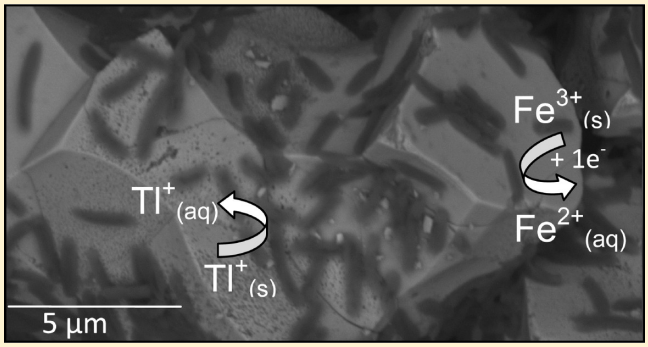

INTRODUCTION

An estimated 2−5 thousand tonnes of thallium (Tl) per year is mobilized worldwide, primarily through the burning of fossil fuels and smelting of ferrous and nonferrous ores.[1] Tl is a priority pollutant and of particular importance because it is highly toxic to biota and studied to a lesser degree than other prominent metals such as arsenic (As), lead (Pb), cadmium (Cd), and mercury (Hg).[1,2] Average Tl concentrations range from 0.17 to 2.8 μg/g in uncontaminated soils, 0.001 to 0.25 μg/L in groundwater, 0.001 to 0.036 μg/L in lake water, and 0.012 to 0.016 μg/L in seawater.[2,3] Elevated Tl concentrations are reported in soils (125 mg/kg), surface waters (534 μg/L), groundwater (1100 μg/L), postmining waste heap (43 mg/kg), and in plants (65 mg/kg) at several historical and current mining sites.[1,4−11] As a chalcophile, Tl is a trace constituent of most zinc (Zn) sulfides (~2.2 μg/g); consequently, U.S. electrolytic Zn and Cd plants generate an estimated 3.1 tonnes of Tl per year in solid and liquid wastes.[12,13] Zn concentrates contain 20−100 mg/L Tl which codeposits with Zn during electrolysis and is removed during processing to less than 5 mg/L Tl to avoid contamination.[13] The Zn industry uses the Jarosite process to eliminate iron (Fe) and other impurities such as Tl and Pb through precipitation of a jarosite compound, $(AFe_3(SO_4)_2(OH)_6)$, where A sites are occupied by monovalent (e.g., K^{1+}) and divalent cations (e.g., Pb^{2+}).[14] Jarosite precipitation is used in 80% of world Zn production (8 Mt Zn/year) and advantageous because it is easily filtered and economical and gives low losses of Zn metal. K−jarosite is the most thermodynamically stable jarosite compound, yet Tl is extensively incorporated into K−jarosite when present in synthesis solutions and will preferentially precipitate relative to ammonium or sodium jarosite.[13]

While naturally occurring Tl−jarosites are rarely reported, a Tl−jarosite analogue, dorallcharite $(Tl_{0.8}K_{0.2}Fe_3(SO_4)_2(OH)_6)$, was identified on the surface of Tl-rich sulfide ores in Macedonia.[15] The low natural concentrations and historically poor analytical sensitivity of Tl coupled with the use of conventional bulk analytical methods such as X-ray diffraction (XRD) may preclude identification of Tl−jarosite in the environment. Nevertheless, Tl−jarosite is expected to form under oxidizing, ferric-rich, and acidic (pH < 3) environments.[13,15,16] The stability of jarosite is limited by conversion above pH 4−5 to goethite or metastable phases such as schwertmannite or ferrihydrite. Despite the importance of jarosite precipitation for Tl control in the Zn industry and the potential for Tl−jarosite formation under acid mine drainage conditions, very little is known about the mobilization of Tl from these phases. This issue is further exacerbated by the large quantities of jarosites produced in the Zn industry; for example, a plant annually producing 150 000 tonnes of metallic Zn will

Received: June 7, 2012
Revised: August 31, 2012
Accepted: September 19, 2012
Published: September 19, 2012

generate 125 000 tonnes of jarosite.[14] The most widely used disposal method is in lined ponds under circumneutral conditions. Under these conditions, aqueous Tl(I) is predicted to dominate over Tl(III) due to the high reduction potential ($E°$ = +1.28 V) for the Tl(III)/Tl(I) redox couple.[11,17] However, thermodynamic predictions of Tl speciation versus field measurements have yielded contradictory results.[17] As expected, aqueous Tl(I) dominated (>98%) river waters downstream from an abandoned Pb−Zn mine in Southern France.[11] On the other hand, aqueous Tl(III) complexes dominated (68%) water samples taken from the Great Lakes due to Tl(I) oxidation by planktonic bacteria.[18,19] Tl(I) is also unique compared to many aqueous metals such as Pb or As because it does not sorb significantly to iron oxides yet may be immobilized as a Tl_2O_3 precipitate via oxidation of Tl(I) to Tl(III) on the surface of Mn−oxides.[11,20,21]

Determining the biogeochemical stability of jarosites is important to evaluate the potential mobility of metals such as Tl from jarosite disposal sites. Due to the increasing awareness of Tl contamination in countries such as China, Tl is quickly emerging as a pollutant of concern, yet the potential influence of bacteria on Tl mobility remains unknown.[3,22,23] Tl binds to the sulfhydryl groups of proteins and inhibits a variety of enzymatic reactions, and due to the nondiscriminatory uptake of Tl(I) over K(I), Tl(I) will also interfere with a range of K-dependent processes such as (Na/K)-ATPase synthesis.[24] Accordingly, Tl(I) inhibited growth in *Saccharomyces cerevisiae*, *Escherichia coli*, and *Bacillus megaterium*, while increased aqueous K concentrations alleviated Tl toxicity in *S. cerevisiae* and *B. megaterium*.[25] Similarly, increased intracellular Tl accumulation decreased intracellular K accumulation in the cyanobacterium *Synechocystis* PCC 6803.[26] The toxicity of Tl is also dependent on oxidation state; for example, Tl(III) was 50 000-fold more toxic than Tl(I) to the unicellular green algae *Chlorella*.[27] Biomethylation of Tl was also shown in a mixed bacterial culture isolated from sewage sludge in lake sediment under anaerobic conditions.[28]

Despite the environmental relevance of Tl and jarosites, few studies have focused on the abiotic and biotic dissolution of jarosites under anaerobic circumneutral conditions with even fewer studies focused on general Tl biogeochemistry.[28−39] Therefore, the objectives of this study were to (1) assess the effects of the model metal reducing bacterium, *Shewanella putrefaciens* CN32, on the reductive dissolution of synthetic Tl−jarosite under circumneutral anaerobic conditions and (2) evaluate the fate and toxicity of Tl on *S. putrefaciens* CN32.

S. putrefaciens CN 32 was chosen because it is a model−subsurface bacterium, originally isolated from a subsurface core sample (250 m) obtained during the drilling of a shale−sandstone sequence in northwestern New Mexico.[40] As a facultative anaerobe, *S. putrefaciens* has shown remarkable anaerobic versatility and is capable of reducing a variety of terminal electron acceptors such as As, U, Fe, and Pu (see 40 and references therein).[41,42]

MATERIALS AND METHODS

Preparation of Tl−Jarosite/Cell Suspensions and Sampling Protocol. Tl(I) jarosite was synthesized using ACS-grade reagents according to the method outlined by Dutrizac (1997) with the resulting chemical formula $(H_3O)_{0.29}Tl_{0.71}Fe_{2.74}(SO_4)_2(OH)_{5.22}(H_2O)_{0.78}$[13,43] (see Supporting Information Section 1 for more details). *Shewanella putrefaciens* CN 32 cultures (ATC# BAA-453) were prepared from 1.5 mL of frozen glycerol stocks maintained at −80 °C and were , harvested, and transferred into a modified M1 minimal media (Supporting Information Section S2). The inoculated media was divided, and one portion was autoclaved to serve as a heat-killed experimental control. All solutions were prepared from ACS-grade reagents and either filter sterilized (0.2 μm) or autoclaved.

Minimal media was transferred to an anaerobic chamber (95% N_2/5% H_2), and 15 mL aliquots were dispensed into 20 mL polypropylene test tubes containing 0.0561 ± 0.0097 g of Tl−jarosite. Sample treatments varied based on the presence and/or viability of *S. putrefaciens* and contained either (a) no cells (48 samples), (b) viable cells (48 samples), or (c) autoclaved cells (18 samples). Additional sets of controls containing only minimal media were prepared to examine background pH, Eh, ATP, and elemental concentrations over time in the absence of Tl−jarosite and contained either (a) no cells (8 samples) or (b) viable cells (8 samples). All samples were capped, sealed with parafilm, covered with aluminum (Al) foil, rotated end-over-end at 20 rpm in the anaerobic chamber using a benchtop rotator (Glas-Col) at 28 °C, and sampled at selected time intervals. Samples containing Tl−jarosite were sampled in triplicate, while minimal media controls (i.e., no Tl−jarosite) were sampled in duplicate.

All samples were monitored for pH (Thermo Ross Sure-flow semi micro pH probe) and Eh (Thermo Ross Sure Flow combo redox/ORP) at each sampling interval. Slurries from each sample were collected at selected time intervals and imaged using field emission-environmental scanning electron microscopy (FE-ESEM, FEI-Quanta 200F) (Supporting Information Section S3). Microbial metabolism was monitored using the Promega BacTiter-Glo Microbial Cell Viability Assay, a rapid and sensitive ATP-based luminescent technique. A slurry (1.0 mL) from each sample was collected and divided into two aliquots. To avoid an overestimation of intracellular ATP, extracellular and intracellular (i.e., microbial) ATP were separated by filtration through a 0.1 μm syringe filter (Millex-VV, Millipore) and analyzed separately using the same analytical protocol (Supporting Information Section S4).[44] Intracellular ATP (referred to as ATP_{INT}) was calculated by subtracting extracellular ATP from total ATP. Starting ATP concentrations were converted to cell counts using an average ATP-per-biovolume concentration of 1.75×10^{-10} nmol/cell ATP, and the starting cell concentration was 1.3×10^8 cells/mL.[44]

The remaining sample was syringe filtered (0.20 μm), and a subsample (100 μL) of the filtrate was analyzed immediately for Fe(II) and total Fe concentrations via the Ferrozine method as described by Viollier et al. (2000).[45,46] The remaining filtrate was diluted and acidified with doubly distilled 0.016 M HNO_3 and stored at 4 °C until analysis. Aqueous concentrations of Tl, Fe, S, and all minimal media components (i.e., K, Mg, etc.) of the stored samples were determined using inductively coupled plasma optical emission spectroscopy (ICP-OES).

Tl Sorption and Toxicity Experiment. To evaluate Tl toxicity and the potential for Tl sorption onto *S. putrefaciens* cells, a solution of reagent-grade Tl_2SO_4 (80 mM) was added to suspensions of living and autoclaved bacteria dispersed in 0.1 M NaCl to give a final concentration of 35 μM Tl and sampled over time (0, 24, 72 h). Additional cell-free controls were prepared to examine the potential for abiotic Tl removal via precipitation. The pH was adjusted to pH 5 and 6.2 using 0.1 M HCl. The pHs were chosen to reflect the final pH of the biotic experiment (pH 6.30) and examine changes in Tl sorption at a lower pH (pH 5).

Peter et al. (2007) showed optimal Tl adsorption onto *Aspergillus niger* between pH 4 and 5.[47] The initial and final pH values were measured, and ATP_{INT} concentrations were determined (Supporting Information Section S4). Samples were filtered through a 0.1 μm syringe filter (Millex-VV, Millipore) and analyzed for aqueous Tl concentrations using ICP-OES. Initial cell concentrations were 0.265 mg_{dw} mL^{-1} (4.0×10^8 cells/mL), and cell growth was also monitored by measuring the cultures' optical density at 600 nm.[44]

RESULTS AND DISCUSSION

Tl Sorption Experiment. Batch sorption tests were conducted to compare Tl removal from solution in autoclaved cells, viable cells, and Tl-spiked media control samples in the absence of Tl–jarosite over 72 h at pH 5 and 6.3. Differences between initial and final aqueous Tl concentrations were compared between the three treatments and showed no significant statistical difference after 72 h at pH 5 (ANOVA, $F = 0.05$, $p = 0.948$) and 6 (ANOVA, $F = 1.33$, $p = 0.333$) (Supporting Information Table S1). Tl sorption onto *S. putrefaciens* biomass may be undetectable due to the low mass of *S. putrefaciens* (dry weight 0.265 mg/mL, 4.0×10^8 cells/mL) chosen to correspond with bacterial concentrations used in the Tl–jarosite experiment. Despite low cell concentrations, Norris et. al (1976) showed Tl(I) uptake in similar cell concentrations of *E. coli* (dry weight 0.40 mg/mL) at higher Tl concentrations (100 μM).[25] Aside from differences in bacterial species, the lack of detectable Tl sorption onto *S. putrefaciens* over *E. coli.* may also be due to environmental redox conditions. Haas et al. (2004) showed decreased molar site concentrations of functional groups in *S. putrefaciens* 200R under anaerobic conditions and suggested *S. putrefaciens* may be a poorer adsorptive agent under anaerobic conditions.[48] Sorption is also not expected to be a significant mechanism for Tl immobilization because Tl(I) does not form strong complexes with ligands due to antibonding electrons in the outer s orbital, particularly with the phosphoryl functional groups expected to dominate at the cell wall at pH 5 and 6.[49]

The toxicity of Tl to *S. putrefaciens* was investigated as a potential obstacle to Tl sorption. Internal ATP concentrations provide a useful indirect metric for microbial biomass estimates in both uncontaminated and metal-contaminated soils, even at high metal concentrations.[50,51] A particular advantage of determining ATP concentrations is the short half life of extracellular ATP released from cells during cell lysis (0.5 h, 16 °C).[52,53] Intracellular ATP (referred to as ATP_{INT} hereafter) concentrations in both treatments at pH 5 decreased to below detection limits within 24 h and showed no significant differences in the decline of ATP_{INT} between control (i.e., no Tl) and Tl-spiked samples (t test, $p = 0.588$) (Figure 1A). By 48 h, samples at pH 6 containing Tl had significantly different ATP_{INT} concentrations than control samples (t test, $p = 0.011$). Irrespective of Tl treatment, differences in pH showed significant differences in ATP_{INT} concentrations within the control (t test, $p = 0.030$) and Tl-spiked (t test, $p = 0.0003$) samples. At 72 h, ATP_{INT} concentrations in pH 6 samples remained detectable (~0.2 nM) and undetectable in pH 5 samples with no significant differences (t test, $p > 0.05$) between ATP_{INT} decline, between 0 and 72 h, between pH regimes or treatments. ATP_{INT} concentrations complemented the $OD_{600\ nm}$ measurements which also showed decreased turbidity over time in all samples (Supporting Information Figure S1). Cell death at pH 5 was attributed to stress associated with the acidic pH rather than Tl toxicity and corroborates previous studies that show low viability

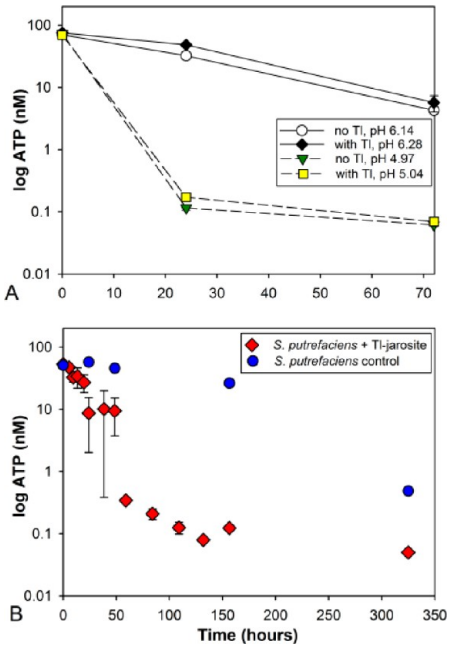

Figure 1. Intracellular ATP concentrations over time in viable (A) *S. putrefaciens* + minimal media in Tl-free and spiked sorption samples at pH ≈ 5 and 6, (B) *S. putrefaciens* control samples (i.e., no Tl–jarosite) and *S. putrefaciens* + Tl–jarosite samples. Note the difference in time scales. Error bars represent standard error ($n = 3$).

of *S. putrefaciens* under low pH (<4) conditions. At pH 6, viability was not related to Tl toxicity and may be due to the lack of nutrients in the NaCl medium. Interestingly, there was greater ATP_{INT} in pH 6 samples containing Tl rather than in the control. The slightly lower pH of the control (6.15) versus the Tl-spiked (6.28) samples may have contributed to decreased viability.

Previous studies demonstrated rapid and active Tl uptake/efflux in fungal and bacterial biomass related to substitution of Tl(I) over K(I) in cellular Na/K-ATPase transport systems due to the greater electronegativity of Tl (1.62) versus K (0.82).[25] Accordingly, Tl toxicity may be reduced by increasing the K:Tl ratio to suppress Tl uptake. Hassler et al. (2007) showed decreased Tl(I) toxicity in the microalga *Chlorella* sp. by increasing K concentrations to an excess of 40–160 times that of Tl which suppressed intracellular Tl accumulation.[54] Inhibition of Tl uptake by K could be particularly important for Tl–jarosite disposal because it is expected to coprecipitate with K–jarosite and the simultaneous release of K and Tl during dissolution may serve to decrease toxicity in biota. Alternatively, depending on the sorptive capacity of the microbial community, high concentrations of K may also serve to reduce uptake in native bacteria and potentially increase Tl mobility.

Tl–Jarosite Control Samples. Aqueous Fe(II) (D.L. = 9.6 μM), Fe_{TOT} (D.L. = 0.04 μM), and Tl (D.L. = 0.08) concentrations were below analytical detection limits (D.L.) in both sterile and inoculated minimal media samples (i.e., in the absence of Tl–jarosite) and remained buffered at pH 7.2 throughout the experiment. Sulfate release over time could not be used to evaluate Tl–jarosite dissolution due to the background contribution of S (34 mM) by the PIPES buffer which destabilizes upon acidification of samples during ICP-OES preparation and contributes to higher sulfate concentrations during analysis.[55] In cell-free and autoclaved cell Tl–jarosite samples, total Fe_{aq} (ICP-OES) concentrations remained below the detection limits of the Ferrozine method and were between 3

and 5 uM (ICP-OES, DL= 0.04 μM) for the duration of the experiment (data not shown).[46] Low Fe concentrations in the control samples were consistent with minimal Fe concentrations observed during K, Pb, As, and Pb–As jarosite dissolution and attributed to the low solubility of Fe(III) at circumneutral pH.[29−31]

Aqueous Tl release from Tl–jarosite was linear in both control treatments and 3.25 times slower in samples containing autoclaved cells (0.20 ± 0.18 μM·h^{-1}, r^2 = 0.955) than in cell-free samples (0.65 ± 0.29 μM·h^{-1}, r^2= 0.966) (Figure 2). At the

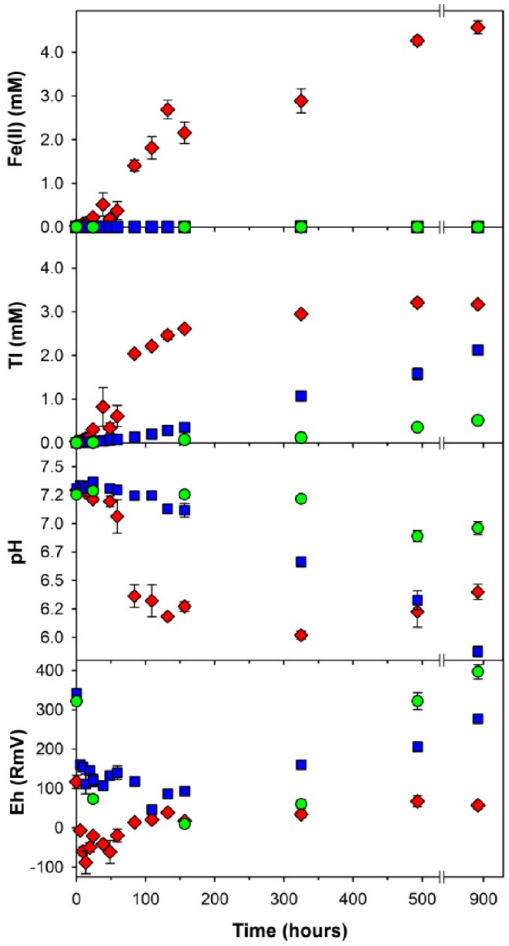

Figure 2. Eh, pH, Fe(II)$_{(aq)}$ production, and Tl$_{(aq)}$ release over time in viable *S. putrefaciens* (red diamonds), cell-free (blue squares), and autoclaved *S. putrefaciens* (green circles) Tl–jarosite samples. Error bars represent standard error (n = 3).

termination of the experiment, final Tl$_{(aq)}$ concentrations were 0.5 ± 0.1 (n = 3) and 2.1 ± 0.1 mM (n = 3) in autoclaved cell and cell-free samples, respectively. Sorption onto autoclaved *S. putrefaciens* was discounted as a possible sink for Tl because *S. putrefaciens* did not show significant Tl uptake in the sorption experiment (Supporting Information Table S1). Attraction between the cell and the jarosite surface was not considered in this study, yet previous electrophoretic mobility measurements of K–jarosite in 0.01 M NaCl revealed two isoelectric points (pH$_{IEP}$): 3.9 and 5.7 with a zeta potential of ~10 mV at pH 7.[56] Between the isoelectric points, jarosite was electronegative, which the authors inferred to be the result of iron(III) hydroxide formation. However, the jarosite surface was electropositive below pH 3.9 and above pH 5.7. Chubar et al. (2008) measured pH$_{IEP}$ ≈ 4 in both autoclaved and viable *S. putrefaciens* CN32 cells in 0.1 M NaCl with at zeta potential of ~18 mV at pH 7.[57] Therefore, decreased dissolution of samples containing autoclaved cells may be related to the electrostatic surface attraction between the negatively charged cell surface of dead *S. putrefaciens* cells with the positively charged Tl–jarosite surface. This attraction may serve to passivate the mineral surface by reducing the Tl–jarosite surface area available for dissolution. However, in the absence of electrophoretic measurements in our study, the mechanism remains to be elucidated and the comparison to other studies should be interpreted cautiously due to the differences in jarosite phases and experimental conditions. Aqueous Tl concentrations of cell-free samples were higher than mass-normalized K concentrations (~1.5 mM) reported by Smith et al.[31] during the unbuffered abiotic dissolution of K–jarosite and is likely a reflection of the structural strain imposed by the larger Tl(I) ion in the jarosite structure expected for alkali site (A-site) substitutions.[13] Substitution of Tl (1.49 Å) versus K (1.33 Å) expands the structural c parameter of the crystal lattice, resulting in the largest known interlayer spacing in the alunite–jarosite family, thereby decreasing the stability of Tl–jarosite over K–jarosite.[13,15,58]

A distinctive color change typically associated with iron hydroxide formation was observed in cell-free control samples, whereby the original yellow Tl–jarosite changed to a reddish hue at 132 h and darkened to a deep red by termination of the experiment (Supporting Information Figure S2).[59] BSE-SEM images of the cell-free Tl–jarosite surface showed extensive pitting after 168 h (Supporting Information Figure S3 A-C) and channelling (Supporting Information Figure S2B) at 893 h similar to surface textures observed during K–jarosite dissolution.[60] Over time, SEM images show a gradual comminution of cell-free samples (Figure 3B and 3D) and extensive secondary mineralization characterized as spherical precipitates (Supporting Information Figure S3D) similar to those identified as goethite during dissolution of Pb and K–jarosite.[30,58] Mineral saturation indices were calculated by the React program within the Geochemist's Workbench (GWB, version 7.01) using solution chemistry at 893 h (Supporting Information Table S2) and predicted the precipitation of hematite > schwertmannite > goethite > Fe(OH)$_3$ (Supporting Information Table S3). Hematite was discounted because it is expected to form over longer durations at circumneutral pH.[61] Energy-dispersive X-ray (EDX) spectra of a representative secondary precipitate at 893 h taken away from the original Tl–jarosite shows the presence of Fe (25 At %) and O (75 At %), potentially confirming formation of an Fe oxide (Supporting Information Figure S4).

Predicted formation of goethite or Fe(OH)$_3$ is important because iron oxides are common minerals in soils and colloids in aquatic environments and exert significant control over the concentrations and speciation of trace elements such as Pb, As, and Cd.[20] For example, during the abiotic dissolution of Ag and Pb–jarosite, Ag and Pb concentrations were below detection limits and were either sorbed or coprecipitated with Fe–oxides.[29,32,62] In contrast, Tl(I) is highly soluble and has a low affinity for hydrous ferric oxides. Jacobsen et al. (2005) reported 1.5% Tl versus 100% Ag sorption onto ferrihydrite at pH 7.[11,62,63] Upon the basis of atomic radii and oxidation state, one may expect similar iron hydroxide surface complexation mechanisms for monovalent Ag (1.31 Å) and Tl (1.49 Å). However, given the electron configuration of Tl(I): ([Xe] 4f^{14}5d^{10}6s^2), the 6s orbital electrons are σ-antibonding whereas the two electrons in 4d$_{z2}$ orbital of Ag(I):([Kr]4d^{10}) move to the empty 5s orbital to form

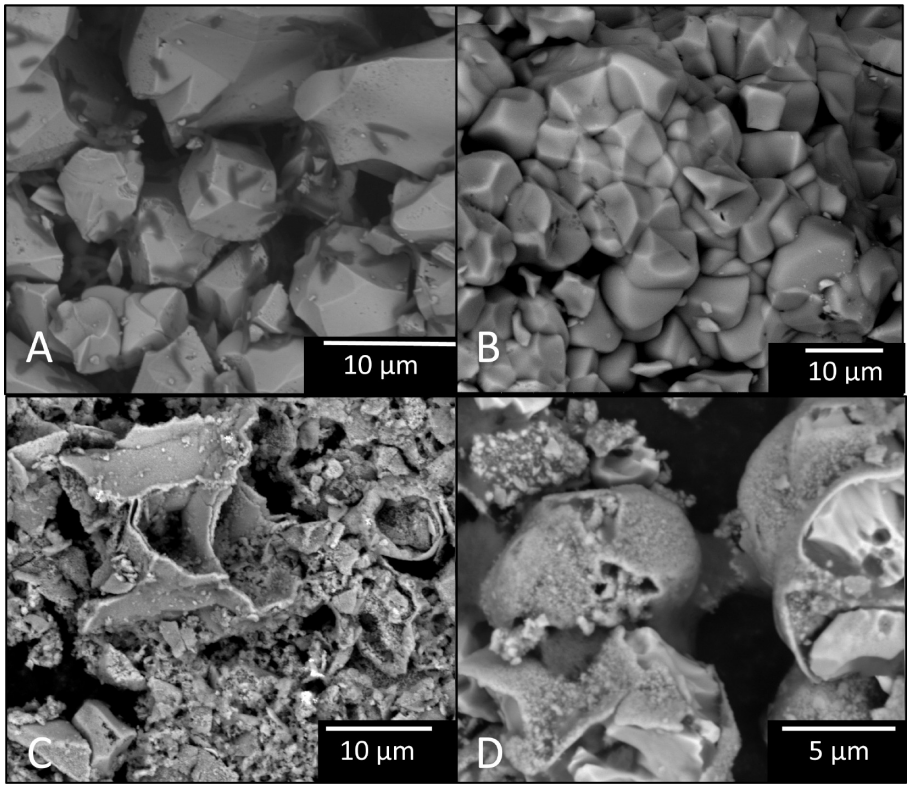

Figure 3. Backscattered-electron (BSE) image of the inoculated (viable) Tl–jarosite samples at (A) 0 and (C) 893 h and the control (cell-free) Tl–jarosite samples at (B) 0 and (D) 893 h.

relatively strong bonds with surface complexes.[63] Liu et al. (2011) showed 35.4–78.5% Tl sorption onto goethite and suggested that increased Tl sorption may also be related to the differences of surface structure and crystallinity between ferrihydrite and goethite.[64]

To account for the high concentrations of Tl observed in this experiment, the React program (GWB) was used to predict the speciation of aqueous and sorbed Tl. The Dzombak and Morel (1990) diffuse layer complexation model (DLM) was incorporated into the reaction model, and the database was amended to include surface complexation constants for weak (log K_{ads}= −2.67) and strong (log K_{ads}= −3.76) >FeOTl sites.[11] Using solution data collected at 893 h, React predicted that 8.0% and 0.2% of Tl was sorbed to the weak and strong sites of the iron hydroxide, respectively. A small percentage (0.6%) would remain as aqueous TlCl (aq), and 91.2% would dominate as aqueous Tl(I). While thermodynamic modeling was useful to evaluate Tl–jarosite dissolution, the predicted Tl speciation and sorption should be interpreted qualitatively rather than quantitatively because the predictions were not confirmed experimentally and would likely differ due to differences in sorption conditions and solution chemistry. Moreover, at 863 h experimental samples did not reach equilibrium. Nonetheless, the predicted high concentrations of free $Tl^{+}_{(aq)}$ are consistent with field observations and theoretical predictions where the aqueous Tl(I) species dominates in near-neutral pH and low Eh environments.[11,17] On the basis of aqueous Tl data and thermodynamic modeling, Tl did not sorb significantly to the iron oxides predicted to form in this study which even under abiotic conditions may ultimately increase Tl mobility and bioavailability in the environment.[29,30,32]

Microbial Reduction of Tl–Jarosite. Aqueous Fe(III) concentrations remained below detection limits in all Tl–jarosite samples containing viable cells. However, Fe reduction, Fe(II)= 0.032 ± 0.004 mM (n = 3), was observed within the first sampling period and likely occurred in the time between initial inoculation and ferrozine analysis (approximately 1 h) (Figure 2). Early onset of Fe reduction coincided with increased Eh as compared to inoculated minimal media controls where Fe reduction was absent and is presumably due to electron transfer to Fe(III) (Figure 2). Aqueous Fe(II) concentrations increased at a rate of 7.3 ± 2.2 $\mu M \cdot h^{-1}$ (r^2 = 0.866) until steady state was reached at 493 h. Subsequently, aqueous Fe(II) increased minimally from 4.3 ± 0.1 to 4.6 ± 0.2 mM between 493 and 893 h (Figure 2). Maximum Fe(II) concentrations (4.6 ± 0.2 mM) observed in this study were higher than those reported in a similar study using Ag–jarosite (1.7 mM) with similar cell densities of *S. putrefaciens* under comparable conditions.[32] Differences are likely explained by structural differences between Tl–jarosite and Ag–jarosite whereby Tl(I) (1.49 Å) is larger than Ag(I) (1.31 Å) resulting in larger interlayer spacing, thereby increasing solubility. Additionally, *S. putrefaciens* demonstrated Ag(I) reduction to elemental Ag(0) from Ag–jarosite and may have preferentially used Ag as a terminal electron acceptor over Fe(II), thus reducing total Fe reduction.[32]

Initial $Tl_{(aq)}$ release from Tl–jarosite was rapid in samples containing viable *S. putrefaciens* cells (0.019 ± 0.003 $mM \cdot h^{-1}$, r^2 = 0.938) until 156.5 h when concentrations began to plateau and increased gradually from 2.6 ± 0.03 to 3.2 ± 0.07 mM between 156.5 and 893 h, respectively (Figure 2). BSE-SEM images of inoculated samples showed extensive dissolution (Figure 3A, 3C, 4A, and 4B) and secondary mineralization over time (Figure 4C and 4D). Images at 893 h show an electron-dense cubic

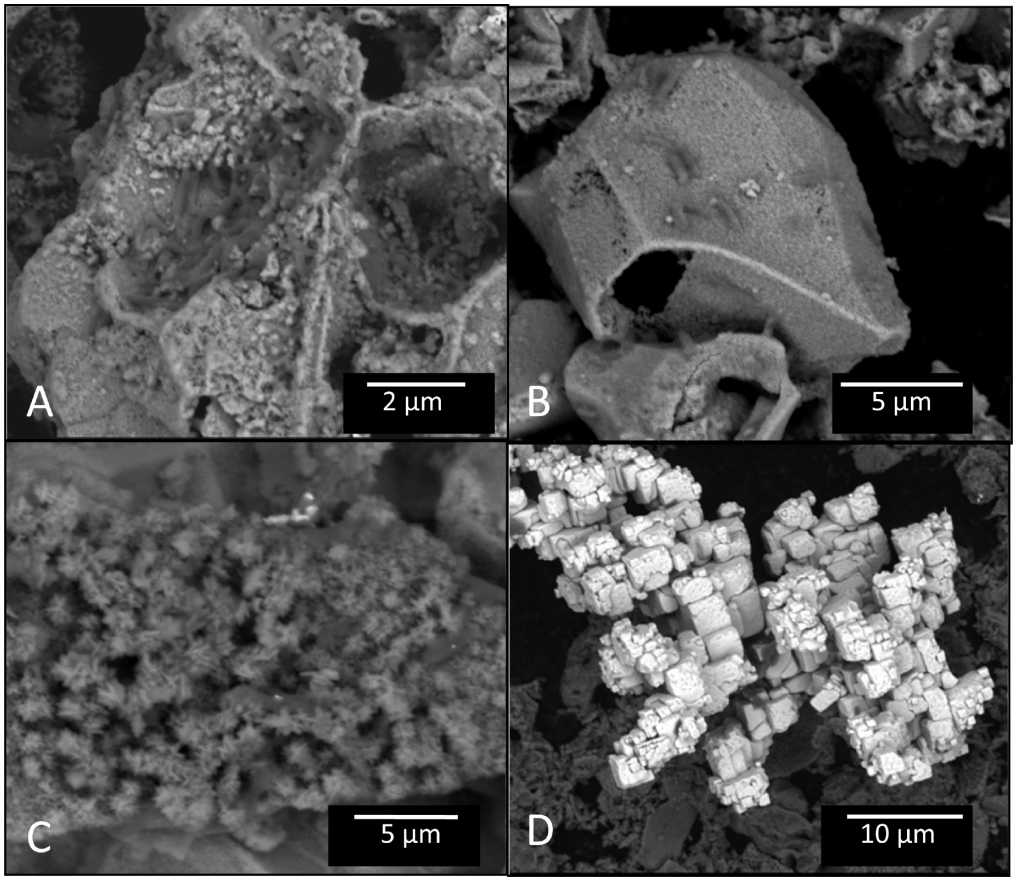

Figure 4. Backscattered-electron (BSE) images taken at 7.5 kV of inoculated Tl−jarosite samples of (A and B) *S. putrefaciens* associated with Tl−jarosite samples at 893 h and secondary precipitates at (C) 493 and (D) 893 h.

secondary precipitate in close proximity to Tl−jarosite, and EDS analysis of the precipitate confirmed the presence of Tl (21 atom %), S (47 atom %), and O (33 atom %) (Figure 4D and Supporting Information Figure S5). The phase is likely Tl(I) sulfate (Tl_2SO_4), and the nonideal stoichiometry of the precipitate is attributed to the elemental signature from the underlying Tl−jarosite and the uncertainties associated with EDS measurements. Upon the basis of the lack of Tl uptake by *S. putrefaciens* in the sorption experiment, it is unlikely that Tl sorption onto *S. putrefaciens* is a significant Tl sink during reductive dissolution of Tl−jarosite.[25,47]

The largest variation of ATP_{INT} (10 ± 9.7 nM) in the Tl−jarosite samples was at 38.5 h and coincided with the largest variations in aqueous Tl (0.86 ± 0.42 mM) and Fe(II) (0.52 ± 0.27 mM) concentrations. At this time interval, the greatest decrease in ATP concentrations occurred in replicates containing the highest Tl and Fe concentrations (Figure 1B). During the Tl sorption experiment, a subsample of viable cells was exposed to a similarly high concentration of Tl (2.5 mM) encountered in this experiment at pH 6.65 and the ATP concentrations were measured immediately in order to track the ratio of extracellular ATP to total ATP. The ratio of filtered to total ATP was 0.69 ± 0.05 (data not shown) at time 0, which corresponds to only 31% ATP_{INT} associated with intracellular (viable) ATP as compared to >99% intracellular ATP (data not shown) associated with *S. putrefaciens* at the low Tl concentration (35 μM) in the sorption experiment. Therefore, high Tl concentrations likely resulted in substantial decreased cell viability. Despite the potentially low viabilityof *S. putrefaciens*, Fe reduction continued until sometime between 325 and 493 h.

On the basis of aqueous Fe(II) and Tl concentrations, samples reached equilibrium between 493 and 893 h. Equilibrium concentrations of Tl, Fe(II), pH, and Eh at 893 h were used to predict saturation indices (log Q/K). Ratios of Fe(II) to acetate, sulfate, and bicarbonate were used to estimate equilibrium concentrations (Supporting Information Table S2). During the reaction, the electron donor (as lactate, $C_3H_5O_3^-$) supplied to *S. putrefaciens* in the minimal media was oxidized, thereby liberating electrons for Fe reduction by the following reaction

$$(H_3O)_{0.29}Tl_{0.71}Fe_{2.74}(SO_4)_2(OH)_{5.22}(H_2O)_{0.78(s)} + 0.68C_3H_5O_3^-{}_{(aq)} + 1.5H^+{}_{(aq)} \rightarrow 0.68CH_3COO^-{}_{(aq)} + 0.68HCO_3^-{}_{(aq)} + 0.71Tl^+{}_{(aq)} + 2.74Fe^{2+}{}_{(aq)} + 2SO_4^{2-}{}_{(aq)} + 4.92H_2O_{(l)} \quad (1)$$

The React program (GWB) predicted formation of hematite > magnetite > goethite (Supporting Information Table S4). Hematite was discounted because it is expected that a Fe(II) phase will form. While the particle morphology is characteristic of the "pincushion" morphology associated with schwertmannite (Figure 4A), EDX analysis of 2 of these locations shows low concentrations of sulfur (2−3%) and enrichments in Fe and O (Supporting Information Figure S6). Given the dark brown color change (Supporting Information Figure S2), pH and redox conditions (Figure 2), and morphology [65] the phase is likely a

magnetite precursor such as lepidocrocite.[66] Due to the lack of equilibrium constants for Tl adsorption onto Fe(II) minerals, sorption could not be modeled. However, based on SEM observations, it is expected that secondary precipitation of a Tl(I) precipitate such as at the Tl(I) sulfate observed in this study (Figure 4A) and is likely the most important sink for Tl during dissolution of Tl−jarosite.

Influence of pH. Due to the instability of jarosite minerals at circumneutral pH and production of H^+ observed during dissolution in previous studies, decreases in pH may also be used as a proxy for jarosite dissolution.[30,31,33] The pH of the cell-free and inoculated minimal media control samples (i.e., no Tl−jarosite) in this study remained buffered at pH 7.3 throughout the experiment (Figure 2). Between 156.5 and 325 h, the buffering capacity of the cell-free Tl−jarosite samples was exceeded and the pH decreased from 7.12 ± 0.06 to 6.66 ± 0.04 and to 5.88 ± 0.05 at 893 h. The decrease in pH is reflective of the increased acidity associated with jarosite dissolution, consistent with previous abiotic dissolution studies of buffered (Ag) and unbuffered (K, Pb−As) jarosites, and described by the following reaction[30−32]

$$(H_3O)_{0.29}Tl_{0.71}Fe_{2.74}(SO_4)_2(OH)_{5.22}(H_2O)_{0.78} + 1.93H_2O \rightarrow 2.74Fe(OH)_3 + 0.71Tl^+ + 2SO_4^{2-} + 3.29H^+ \quad (2)$$

The pH of Tl−jarosite samples containing autoclaved cells did not exceed the buffering capacity of the media and decreased minimally from 7.25 ± 0.01 at 0 h to 6.96 ± 0.06 by 893 h. The buffering capacity of the minimal media was exceeded earlier in Tl−jarosite samples containing viable cells as compared to cell-free samples. Between 59 and 84 h, the pH decreased from 7.06 ± 0.15 to 6.36 ± 0.10 and reached the lowest pH value of 6.02 ± 0.04 until 325 h followed by an increase to 6.40 ± 0.07 at 893 h (Figure 2).The increase in pH observed later in the inoculated samples was consistent with previous magnetite formation by *S. putrefaciens*. The pH buffering effect by *S. putrefaciens* CN 32 the result of HCO_3^- production and H^+ during the Fe reduction (eq 1). According to eqs 1 and 2, abiotic dissolution of jarosite may have a greater impact on the acidity released during Tl−jarosite dissolution and may be buffered by microbial processes via Fe reduction.

Environmental Implications. The decrease in pH and increase in aqueous Tl concentrations over time in the cell-free Tl−jarosite dissolution studies demonstrate that Tl−jarosite is susceptible to significant incongruent dissolution under abiotic conditions. However, Tl−jarosite dissolution may be enhanced through the microbial reduction of structural Fe. The major difference between each regime is related to the secondary Fe mineralization (i.e., Fe(II) versus Fe(III)) associated with dissolution, and the role secondary precipitates may play to sequester Tl remains to be elucidated. Given the conservative chemical nature of Tl demonstrated in both experiments, Tl may remain soluble under circumneutral to acidic anaerobic conditions.

The results from this study provide important yet preliminary insights into the fundamental mechanisms governing the abiotic and biotic dissolution of Tl−jarosite and Tl biogeochemistry. The effects of temperature, aqueous phase mixing rate, competing microbial communities, natural organic matter, suspension density, and removal of reaction products on dissolution kinetics were not considered and leaves opportunity for future refinement.[30] The Tl/bacteria sorption experiment was useful to provide a Tl mass balance for results observed in the Tl−jarosite dissolution experiment yet did not provide a comprehensive assessment of Tl sorption onto *S. putrefaciens*. Future studies should consider Tl sorption across a pH range, microbial concentrations, nutritional conditions, and Tl concentrations to elucidate the Tl-detoxification mechanism. Moreover, while *S. putrefaciens* CN32 is a well-characterized, model metal-reducing bacterium, future studies should assess the reductive dissolution of Tl−jarosite using a suite of other environmentally relevant bacteria such as *Geobacter* sp or microbial consortia collected from mine waste repositories to improve our understanding of thallium jarosite solubility.

■ ASSOCIATED CONTENT

Ⓢ Supporting Information

Additional details including synthesis of Tl−jarosite, preparation of *S. putrefaciens* suspensions, ATP and SEM analysis, Tl sorption results, geochemical modeling parameters/results, and SEM-EDS analysis of secondary precipitates. This material is available free of charge via the Internet at http://pubs.acs.org.

■ AUTHOR INFORMATION

Corresponding Author

*Phone: (519) 888-4567 ext. 32820; fax: (519) 746-7484; E-mail: christina.smeaton@uwaterloo.ca, christinasmeaton@gmail.com.

Present Addresses

[‡]Ecohydrology Research Group, Department of Earth and Environmental Sciences, University of Waterloo, Waterloo, Ontario, Canada, N2L 3G1.

[§]Department of Microbiology, University of Tennessee, Knoxville, Tennessee, 37996, United States.

Notes

The authors declare no competing financial interest.

■ ACKNOWLEDGMENTS

We gratefully acknowledge the financial support of NSERC. We also thank Megan Goetz, Candace McCort, Michael Dufour, Nadine Loick, and J. C. Barrette for sample preparation, sampling, and analytical assistance.

■ REFERENCES

(1) Cheam, V. Thallium contamination of water in Canada. *Water Qual. Res. J. Can.* **2001**, *36* (4), 851−878.

(2) Peter, A. L.; Viraraghavan, T. Thallium: a review of public health and environmental concerns. *Environ. Int.* **2005**, *31* (4), 493−501.

(3) Xiao, T.; Yang, F.; Li, S.; Zheng, B.; Ning, Z. Thallium pollution in China: A geo-environmental perspective. *Sci. Total Environ.* **2011**, *421*, 51−58.

(4) Wierzbicka, M.; Szarek-Lukaszewska, G.; Grodzinska, K. Highly toxic thallium in plants from the vicinity of Olkusz (Poland). *Ecotoxicol. Environ. Saf.* **2004**, *59* (1), 84−88.

(5) Xiao, T. F.; Boyle, D.; Guha, J.; Rouleau, A.; Hong, Y. T.; Zheng, B. S. Groundwater-related thallium transfer processes and their impacts on the ecosystem: southwest Guizhou Province, China. *Appl. Geochem.* **2003**, *18* (5), 675−691.

(6) Casiot, C.; Egal, M.; Bruneel, O.; Verma, N.; Parmentier, M.; Elbaz-Poulichet, F. Predominance of Aqueous Tl(I) Species in the River System Downstream from the Abandoned Carnoules Mine (Southern France). *Environ. Sci. Technol.* **2011**, *45* (6), 2056−2064.

(7) Xiong, Y. L. The aqueous geochemistry of thallium: speciation and solubility of thallium in low temperature systems. *Environ. Chem.* **2009**, *6* (5), 441−451.

(8) Cheam, V.; Garbai, G.; Lechner, J.; Rajkumar, J. Local impacts of coal mines and power plants across Canada. I. Thallium in waters and sediments. *Water Qual. Res. J. Can.* **2000**, *35* (4), 581−607.
(9) Lis, J.; Pasieczna, A.; Karbowska, B.; Zembrzuski, W.; Lukaszewski, Z. Thallium in soils and stream sediments of a Zn-Pb mining and smelting area. *Environ. Sci. Technol.* **2003**, *37* (20), 4569−4572.
(10) Martin, F.; Garcia, I.; Dorronsoro, C.; Simon, M.; Aguilar, J.; Ortiz, I.; Fernandez, E.; Fernandez, J. Thallium behavior in soils polluted by pyrite tailings (Aznalcollar, Spain). *Soil Sediment Contam.* **2004**, *13* (1), 25−36.
(11) Casiot, C.; Egal, M.; Bruneel, O.; Verma, N.; Parmentier, M.; Elbaz-Poulichet, F. Predominance of Aqueous Tl(I) Species in the River System Downstream from the Abandoned Carnoules Mine (Southern France). *Environ. Sci. Technol.* **2011**, *45* (6), 2056−2064.
(12) Nriagu, J. O. *Thallium in the environment*; Wiley: New York, 1998.
(13) Dutrizac, J. E. The behavior of thallium during jarosite precipitation. *Metall. Mater. Trans. B* **1997**, *28* (5), 765−776.
(14) Dutrizac, J. E.; Jambor, J. L., Jarosites and their application in hydrometallurgy. *Sulfate Minerals-Crystallography, Geochemistry and Environmental Significance*; The Mineralogical Society of America: Washington, DC, 2000; Vol. *40*, pp 405−452.
(15) Balic Zunic, T.; Moelo, Y.; Loncar, Z.; Micheelsen, H. Dorallcharite, $Tl_{0.8}K_{0.2}Fe_3(SO_4)_2(OH)_6$, a new member of the jarosite-alunite family. *European J. Mineral.* **1994**, *6* (2), 255.
(16) Stoffregen, R.; Alpers, C.; Jambor, J. L. Alunite-jarosite crystallography, thermodynamics, and geochronology. *Rev. Mineral. Geochem.* **2000**, *40* (1), 453.
(17) Xiong, Y. L. The aqueous geochemistry of thallium: speciation and solubility of thallium in low temperature systems. *Environ. Chem.* **2009**, *6* (5), 441−451.
(18) Lin, T. S.; Nriagu, J. Thallium speciation in the Great Lakes. *Environ. Sci. Technol.* **1999**, *33* (19), 3394−3397.
(19) Twining, B. S.; Twiss, M. R.; Fisher, N. S. Oxidation of thallium by freshwater plankton communities. *Environ. Sci. Technol.* **2003**, *37* (12), 2720−2726.
(20) Ponthieu, M.; Juillot, F.; Hiemstra, T.; van Riemsdijk, W. H.; Benedetti, M. F. Metal ion binding to iron oxides. *Geochim. Cosmochim. Acta* **2006**, *70* (11), 2679−2698.
(21) Bidoglio, G.; Gibson, P.; O'Gorman, M.; Roberts, K. X-ray absorption spectroscopy investigation of surface redox transformations of thallium and chromium on colloidal mineral oxides. *Geochim. Cosmochim. Acta* **1993**, *57* (10), 2389−2394.
(22) Peter, A. L. J.; Viraraghavan, T. Thallium: a review of public health and environmental concerns. *Environ. Int.* **2005**, *31* (4), 493−501.
(23) Kazantzis, G. Thallium in the environment and health effects. *Environ. Geochem. Health* **2000**, *22* (4), 275−280.
(24) Peter, A. L. J.; Viraraghavan, T. Thallium: a review of public health and environmental concerns. *Environ. Int.* **2005**, *31* (4), 493−501.
(25) Norris, P.; Man, W. K.; Hughes, M. N.; Kelly, D. P. Toxicity and Accumulation of Thallium in Bacteria and Yeast. *Arch. Microbiol.* **1976**, *110* (2−3), 279−286.
(26) Avery, S. V.; Codd, G. A.; Gadd, G. M. Cesium Accumulation and Interactions with Other Monovalent Cations in the Cyanobacterium *Synechocystis* PCC-6803. *J. Gen. Microbiol.* **1991**, *137*, 405−413.
(27) Ralph, L.; Twiss, M. R. Comparative toxicity of thallium(I), thallium(III), and cadmium(II) to the unicellular alga *Chlorella* isolated from Lake Erie. *Bull. Environ. Contam. Toxicol.* **2002**, *68* (2), 261−268.
(28) Schedlbauer, O. F.; Heumann, K. G. Biomethylation of thallium by bacteria and first determination of biogenic dimethylthallium in the ocean. *Appl. Organomet. Chem.* **2000**, *14* (6), 330−340.
(29) Smeaton, C. M.; Fryer, B. J.; Weisener, C. G. Intracellular Precipitation of Pb by *Shewanella putrefaciens* CN32 during the Reductive Dissolution of Pb-Jarosite. *Environ. Sci. Technol.* **2009**, *43* (21), 8091−8096.
(30) Smith, A. M. L.; Dubbin, W. E.; Wright, K.; Hudson-Edwards, K. A. Dissolution of lead- and lead-arsenic-jarosites at pH 2 and 8 and 20 degrees C: Insights from batch experiments. *Chem. Geol.* **2006**, *229* (4), 344−361.
(31) Smith, A. M. L.; Hudson-Edwards, K. A.; Dubbin, W. E.; Wright, K. Dissolution of jarosite $[KFe_3(SO_4)_2(OH)_6]$ at pH 2 and 8: Insights from batch experiments and computational modelling. *Geochim. Cosmochim. Acta* **2006**, *70* (3), 608−621.
(32) Weisener, C. G.; Babechuk, M. G.; Fryer, B. J.; Maunder, C. Microbial Dissolution of Silver Jarosite: Examining Its Trace Metal Behaviour in Reduced Environments. *Geomicrobiol. J.* **2008**, *25* (7−8), 415−424.
(33) Welch, S. A.; Christy, A. G.; Kirste, D.; Beavis, S. G.; Beavis, F. Jarosite dissolution I - Trace cation flux in acid sulfate soils. *Chem. Geol.* **2007**, *245* (3−4), 183−197.
(34) Welch, S. A.; Kirste, D.; Christy, A. G.; Beavis, F. R.; Beavis, S. G. Jarosite dissolution II-Reaction kinetics, stoichiometry and acid flux. *Chem. Geol.* **2008**, *254* (1−2), 73−86.
(35) Norlund, K. L. I.; Baron, C.; Warren, L. A. Jarosite formation by an AMD sulphide-oxidizing environmental enrichment: Implications for biomarkers on Mars. *Chem. Geol.* **2010**, *275* (3−4), 235−242.
(36) Al, T. A.; Blowes, D. W.; Jambor, J. L.; Scott, J. D. The Geochemistry of Mine-Waste Pore-Water Affected by the Combined Disposal of Natrojarosite and Base-Metal Sulfide Tailings at Kidd Creek, Timmins, Ontario. *Can. Geotech. J.* **1994**, *31* (4), 502−512.
(37) Bridge, T. A. M.; Johnson, D. B. Reductive dissolution of ferric iron minerals by Acidiphilium SJH. *Geomicrobiol. J.* **2000**, *17* (3), 193−206.
(38) Jurjovec, J.; Ptacek, C. J.; Blowes, D. W.; Jambor, J. L. The effect of natrojarosite addition to mine tailings. *Environ. Sci. Technol.* **2003**, *37* (1), 158−164.
(39) Jones, E. J. P.; Nadeau, T. L.; Voytek, M. A.; Landa, E. R. Role of microbial iron reduction in the dissolution of iron hydroxysulfate minerals. *J. Geophys. Res., [Biogeo.]* **2006**, *111*, G1.
(40) Fredrickson, J. K.; Zachara, J. M.; Kennedy, D. W.; Dong, H. L.; Onstott, T. C.; Hinman, N. W.; Li, S. M. Biogenic iron mineralization accompanying the dissimilatory reduction of hydrous ferric oxide by a groundwater bacterium. *Geochim. Cosmochim. Acta* **1998**, *62* (19−20), 3239−3257.
(41) Campbell, K. M.; Malasarn, D.; Saltikov, C. W.; Newman, D. K.; Hering, J. G. Simultaneous microbial reduction of iron (III) and arsenic (V) in suspensions of hydrous ferric oxide. *Environ. Sci. Technol.* **2006**, *40* (19), 5950−5955.
(42) Fredrickson, J. K.; Romine, M. F.; Beliaev, A. S.; Auchtung, J. M.; Driscoll, M. E.; Gardner, T. S.; Nealson, K. H.; Osterman, A. L.; Pinchuk, G.; Reed, J. L.; Rodionov, D. A.; Rodrigues, J. L. M.; Saffarini, D. A.; Serres, M. H.; Spormann, A. M.; Zhulin, I. B.; Tiedje, J. M. Towards environmental systems biology of Shewanella. *Nat. Rev. Microbiol.* **2008**, *6* (8), 592−603.
(43) Kubisz, J. Studies on synthetic alkali-hydronium jarosites. I. Synthesis of jarosite and natrojarosite. *Mineral. Polonica* **1970**, *1*, 47−57.
(44) Hammes, F.; Goldschmidt, F.; Vital, M.; Wang, Y. Y.; Egli, T. Measurement and interpretation of microbial adenosine tri-phosphate (ATP) in aquatic environments. *Water Res.* **2010**, *44* (13), 3915−3923.
(45) Stookey, L. L. Ferrozine - A New Spectrophotometric Reagent for Iron. *Anal. Chem.* **1970**, *42* (7), 779−781.
(46) Viollier, E.; Inglett, P. W.; Hunter, K.; Roychoudhury, A. N.; Van Cappellen, P. The ferrozine method revisited: Fe(II)/Fe(III) determination in natural waters. *Appl. Geochem.* **2000**, *15* (6), 785−790.
(47) Peter, A. L. J.; Viraraghavan, T. Removal of thallium from aqueous solutions by modified *Aspergillus niger* biomass. *Bioresour. Technol.* **2008**, *99* (3), 618−625.
(48) Haas, J. R. Effects of cultivation conditions on acid-base titration properties of *Shewanella putrefaciens*. *Chem. Geol.* **2004**, *209* (1−2), 67−81.
(49) Kaplan, D. I.; Mattigod, S. V. *Aqueous Geochemistry of Thallium*; Wiley: New York, 1998; Vol. *29*, pp 15−30.
(50) Barajas Aceves, M.; Grace, C.; Ansorena, J.; Dendooven, L.; Brookes, P. Soil microbial biomass and organic C in a gradient of zinc concentrations in soils around a mine spoil tip. *Soil Biol. Biochem.* **1999**, *31* (6), 867−876.

(51) Hinojosa, M. B.; Garcia-Ruiz, R.; Carreira, J. A. Utilizing Microbial Community Structure and Function to Evaluate the Health of Heavy Metal Polluted Soils. *Soil Heavy Met.* **2010**, 185−224.
(52) Conklin, A.; MacGregor, A. Soil adenosine triphosphate: extraction, recovery and half-life. *Bull. Environ. Contam. Toxicol.* **1972**, *7* (5), 296−300.
(53) Cowan, D. A.; Casanueva, A. Stability of ATP in Antarctic mineral soils. *Polar Biol.* **2007**, *30* (12), 1599−1603.
(54) Hassler, C. S.; Chafin, R. D.; Klinger, M. B.; Twiss, M. R. Application of the biotic ligand model to explain potassium interaction with thallium uptake and toxicity to plankton. *Environ. Toxicol. Chem.* **2007**, *26* (6), 1139−1145.
(55) Good, N. E.; Winget, G. D.; Winter, W.; Connolly, T. N.; Izawa, S.; Singh, R. M. M. Hydrogen Ion Buffers for Biological Research. *Biochemistry* **1966**, *5* (2), 467−477.
(56) Sadowski, Z.; Polowczyk, I.; Farbiszewska, T.; Farbiszewska-Kiczma, J. Adhesion of jarosite particles to the mineral surface. *Prace Naukowe Instytutu Gornictwa Politechniki Wroclawskiej Konferencje*; Prace Naukowe Instytutu: Wroclaw, Poland, 2001, Vol. *95*, issue 31, pp 93−102.
(57) Chubar, N.; Behrends, T.; Van Cappellen, P. Biosorption of metals (Cu^{2+}, Zn^{2+}) and anions (F^-, $H_2PO_4^-$) by viable and autoclaved cells of the Gram-negative bacterium *Shewanella putrefaciens*. *Colloids Surf., B* **2008**, *65* (1), 126−133.
(58) Smith, A. M. L.; Hudson-Edwards, K. A.; Dubbin, W. E.; Wright, K. Defects and impurities in jarosite: A computer simulation study. *Appl. Geochem.* **2006**, *21* (8), 1251−1258.
(59) Emerson, D. Potential for Iron-reduction and Iron-cycling in Iron Oxyhydroxide-rich Microbial Mats at Loihi Seamount. *Geomicrobiol. J.* **2009**, *26* (8), 639−647.
(60) Gasharova, B.; Gottlicher, J.; Becker, U. Dissolution at the surface of jarosite: an in situ AFM study. *Chem. Geol.* **2005**, *215* (1−4), 499−516.
(61) Ford, R. G.; Bertsch, P. M.; Farley, K. J. Changes in transition and heavy metal partitioning during hydrous iron oxide aging. *Environ. Sci. Technol.* **1997**, *31* (7), 2028−2033.
(62) Dyck, W. Adsorption and coprecipitation of silver on hydrous ferric oxide. *Can. J. Chem.* **1968**, *46* (8), 1441−1444.
(63) Jacobson, A. R.; McBride, M. B.; Baveye, P.; Steenhuis, T. S. Environmental factors determining the trace-level sorption of silver and thallium to soils. *Sci. Total Environ.* **2005**, *345* (1−3), 191−205.
(64) Liu, J.; Lippold, H.; Wang, J.; Lippmann-Pipke, J.; Chen, Y. Sorption of thallium (I) onto geological materials: Influence of pH and humic matter. *Chemosphere* **2011**, *82* (6), 866−871.
(65) Fan, D.; Neuser, R.; Sun, X.; Yang, Z.; Guo, Z.; Zhai, S. Authigenic iron oxide formation in the estuarine mixing zone of the Yangtze River. *Geo-Mar. Lett.* **2008**, *28* (1), 7−14.
(66) Hansel, C. M.; Benner, S. G.; Fendorf, S. Competing Fe(II)-induced mineralization pathways of ferrihydrite. *Environ. Sci. Technol.* **2005**, *39* (18), 7147−7153.